Low-*Z* internal target from a cryogenically cooled liquid microjet source

M. Kühnel [a], N. Petridis [a], D.F.A. Winters [b,c], U. Popp [b], R. Dörner [a], Th. Stöhlker [b,c], R.E. Grisenti [a,b,*]

[a] *Institut für Kernphysik, J.W. Goethe-Universität, Max-von-Laue-Str. 1, 60438 Frankfurt a. M., Germany*
[b] *GSI, Planckstr. 1, 64291, Germany*
[c] *Physikalisches Institut, Ruprecht-Karls-Universität, Philosophenweg 12, 69120 Heidelberg, Germany*

A B S T R A C T

We carried out an extensive investigation on the production of cryogenically cooled liquid hydrogen and helium droplet beams at the experimental storage ring at GSI with the goal to achieve high area densities for these low-*Z* internal targets. Our results show that an area density of up to 10^{14} cm^{-2} is achieved for both light gases by expanding the liquid through sub-10 μm diameter nozzles. The achieved area density is comparable with the previous results for the hydrogen internal target and represents an improvement by about four orders of magnitude for the helium target.

© 2009 Elsevier B.V. All rights reserved.

For the investigation of fundamental processes characterized by tiny cross-sections the use of an internal target usually provides the highest efficiency in terms of the luminosity [1]. Among the many different internal target species employed, the light low-*Z* gases hydrogen (deuterium) and helium play a central role in current nuclear and atomic physics experiments at storage rings. Elastic and inelastic light-hadron scattering provides a powerful method to gain nuclear structure information for both stable and exotic nuclei with fundamental applications in nuclear astrophysics (see, e.g., the technical report of the EXL collaboration [2]). The use of low-*Z* targets in atomic physics experiments greatly enhances the spectroscopic resolution, and, at the same time, improves the ion-beam life time [3]. Relativistic $p\bar{p}$ collisions offer a unique mean to address the fundamental issues of quantum chromodynamics, including the puzzling question on the origin of mass [4].

For many of the above applications besides a large target area density $n\Delta x$ ($10^{13}-10^{15}$ cm^{-2}) also a small interaction length Δx (<5 mm) is mandatory. However, producing a low-*Z* target with these features represents a challenging experimental task. Cluster beams produced by expanding a gas initially at stagnation source conditions (pressure P_0 and temperature T_0) through a pinhole orifice (a "nozzle") into vacuum, owing to their boundary-free and self-replenishing nature, offer significant advantages as an internal target. As a consequence, in the last decade considerable experimental effort has been made to address the internal target feature requirements by means of molecular-beam techniques,

with most of the work dedicated to the hydrogen target [5–9]. A target beam density of up to 2×10^{14} cm^{-2} with $\Delta x \approx 7$ mm has been demonstrated at the ANKE spectrometer at COSY by expanding hydrogen gas at $T_0 \approx 25$ K through a 16 μm-diameter laval-type nozzle [7,9]. An even higher H_2 area density of $\approx 10^{15}$ cm^{-2} with $\Delta x \approx 20$ mm has been recently achieved in a $\overline{P}$ANDA-like geometry under similar source conditions [10]. In contrast, much less experimental data are available for helium. The only value of $\approx 5 \times 10^{10}$ cm^{-2} [8] reported so far is the orders of magnitude below the target area density required for many future nuclear physicsexperiments, thus making their feasibility at least questionable.

One promising approach that aims at further increasing the target density consists in the expansion of the liquid into vacuum using significantly lower source temperatures. In the recent experiments with liquid helium beams an extreme narrowing of the beam angular divergence, by more than two orders of magnitude, was observed by either lowering the source temperature or increasing the source pressure [11]. This behavior was considered the evidence for a continuous transition between cavitation induced fragmentation and Rayleigh breakup of the liquid jet. In the former case an explosive fragmentation of the liquid occurs, delivering a droplet beam with broad distributions of droplet sizes and directions. In the latter case the liquid propagates as a continuous filament until it spontaneously breaks up into a stream of nearly monodisperse droplets [12]. Several groups employed Rayleigh droplet beams as a convenient means to inject into a storage ring a collimated stream of very large frozen hydrogen droplets [13–15]. The possibility to set the beam angular divergence allows, in turn, adjusting the spatial density at some given distance downstream from the nozzle. An average target spatial density in the range $10^{13}-10^{15}$ cm^{-3} can readily be deduced from the measured angular spectra [11].

---

* Corresponding author at: Institut für Kernphysik, J.W. Goethe-Universität, Max-von-Laue-Str. 1, 60438 Frankfurt a. M., Germany.
   E-mail address: grisenti@atom.uni-frankfurt.de (R.E. Grisenti).

Motivated by these experimental studies, we carried out an extensive investigation on the production of cryogenically cooled liquid beams of both hydrogen and helium at the experimental storage ring (ESR) at GSI. The characterization of the liquid target beams at the ESR, i.e., under true storage ring conditions, was largely motivated by the crucial issue on the gas load in the interaction region during ion beam-target beam collisions. From the extensive ultra-intense laser-cluster interaction studies it is known that up to 90% of the laser energy is transferred to the clusters, eventually leading to their complete fragmentation [16]. Since the energies deposited by the relativistic highly charged ions are expected to be comparable in magnitude, the gas load upon droplet fragmentation might significantly affect the ion-beam life time. This gas load turns out to be negligible when standard gas-jet targets are employed [8]. However, the situation may drastically change when significantly larger droplets are produced by expanding the liquid.

The ESR internal target station has been described in detail elsewhere [5]. Briefly, the liquid beam from the nozzle passes through three differentially pumped high vacuum chambers separated by round skimmers before it reaches the interaction region about 0.6 m downstream from the nozzle. The target beam then propagates into a four-stage differentially pumped dump system. For the present experiments the expansion chamber has been modified substantially to accommodate the cryogenically cooled liquid beam source. The latter consists essentially of a compact, about 500 mm long continuous-flow helium cryostat that can be operated at temperatures down to 4 K. The source temperature could be stabilized at the desired T_0 by a commercial regulator within 0.02 K or better. The cryostat was mounted on a three-dimensional translational stage driven by stepping motors in the x and y directions to allow for a precise beam alignment with the skimmers along the z axis. Commercial electron microscope apertures were used as nozzles. In order to make the liquid beam compatible with the ultra-high vacuum conditions in a storage ring, nozzles with a diameter d_0 of 5 and 3 μm have been used during the experiments. The nozzle plate was mounted onto a home-made copper holder screwed into the end plate of the cryostat. The highly purified (99.9999%) hydrogen or helium gas passed a sequence of three low temperature sintered filters before admission to the source to prevent clogging. The liquified gas was injected into a vacuum chamber pumped by a 1800 l/s turbo pump. Owing to the limited available space on the top of the internal target station the turbo pump was connected to the main expansion chamber by a 375 mm long, 60 × 240 mm rectangular tube that reduced the gas flow rate to an effective pumping speed of ≈ 800 l/s, providing a source chamber pressure ≲ 5 × 10⁻³ mbar for both the hydrogen and the helium target beams.

Neglecting beam losses, e.g., due to evaporation or scattering off the wall's edges, the target particle flow rate in the interaction region $\dot{N} = nv\pi(\Delta x)^2/4$, where n is the particle density and v is the liquid beam velocity, must coincide with the PV-flow through the dump system intake's port $\dot{Q} = S_{dump}P_{dump}$, where S_{dump} is the pumping speed at the dump pressure P_{dump}. With $PV = NkT$ the target area density can be written as

$$n\Delta x = C\frac{P_{dump}}{v} \tag{1}$$

where $C = 4S_{dump}/(\pi kT\Delta x)$. In the present case $S_{dump} = 1050$ l/s for hydrogen and $S_{dump} = 1320$ l/s for helium. For a liquid expansion through a pinhole orifice the beam velocity is given by the Bernoulli expression [11,17]

$$v = \sqrt{\frac{2P_0}{\rho}} \tag{2}$$

where $\rho(P_0, T_0)$ is the liquid density at the specific source pressure and temperature. The target beam spread in the interaction region Δx is set by the current skimmer geometry, and is equal to about 5 mm [5]. This has been confirmed during the present experiments by high-resolution optical detection of the fluorescence light emitted during the interaction with a 150 MeV/u Xe⁵⁴⁺ beam. The EM-CCD camera, coupled to a far-field objective, was placed at an observation angle of 35° with respect to the ion-beam direction. Fig. 1 shows a typical image taken from an extensive series of measurements with both hydrogen and helium beams in a wide range of stagnation source conditions, suggesting a white spot size of $\Delta x \approx 5$ mm. This corresponds to a target beam angular distribution with a FWHM larger than about 10 mrad.

Fig. 2 summarizes the measured area densities as determined from the ESR dump pressure for the hydrogen (Figs. 2(a) and (b)) and helium (Figs. 2(c) and (d)) beams. For a given choice of the source pressure P_0 and temperature T_0 the dump pressure P_{dump} was time-averaged over at least 300 s. For all the stagnation source conditions investigated here the liquid hydrogen and helium densities in Eq. (2) were available in tabular form [18]. Figs. 2(e) and (f) show the pressure–temperature phase diagram of hydrogen and helium, respectively. In almost all the experiments with hydrogen the H_2 gas was expanded from stagnation source conditions falling in the liquid phase, as explicitly indicated by the dotted arrows in Fig. 2(e), whereas the initial helium pressure and temperature correspond to the two-phase supercritical region for $T_0 \gtrsim 5.5$ K (Fig. 2(f)). According to the earlier experimental work with helium droplet beams [19], the helium beam velocity under these steady-state conditions is expected to be higher by up to a factor 2 than that predicted by the Bernoulli formula, Eq. (2). Accordingly, the target densities displayed in Figs. 2(c) and (d) are eventually overestimated by the same factor for source temperatures above about 5.5 K.

One can see from Figs. 2(a) and (b) that the hydrogen area density rapidly increases by decreasing the source temperature, and reaches the largest value of $\approx 10^{14}$ cm⁻² at $P_0 = 40$ bar and $T_0 = 27$ K, measured with the 3 μm diameter nozzle. The data for He (Figs. 2(c) and (d)) clearly show a similar, nearly exponential increase in the area density for source temperatures below about 6 K, up to a maximum value of $\approx 10^{14}$ cm⁻² at $P_0 = 10$ bar and $T_0 = 4.8$ K, as seen in Fig. 2(c). Since the hydrogen and helium
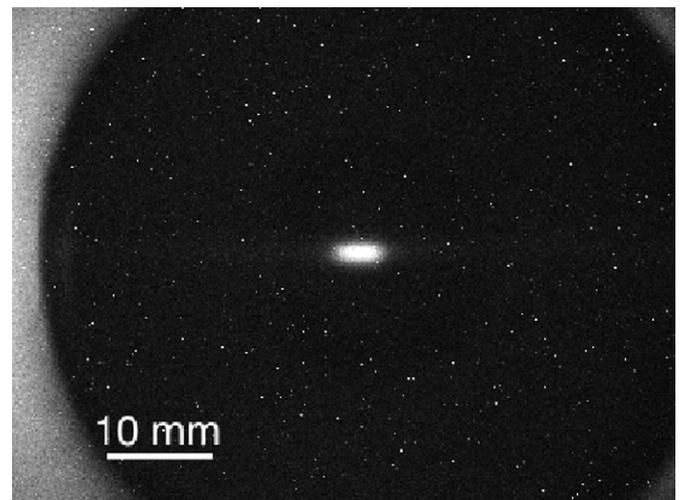
Fig. 1. Image showing the overlap region (the white spot visible in the middle) between the hydrogen target beam (propagating from the top to the bottom in the figure) and the about 3 mm wide 150 MeV/u Xe⁵⁴⁺ ion beam, recorded with an EM-CCD camera located at an observation angle of 35° with respect to the ion-beam direction (from the right to the left).
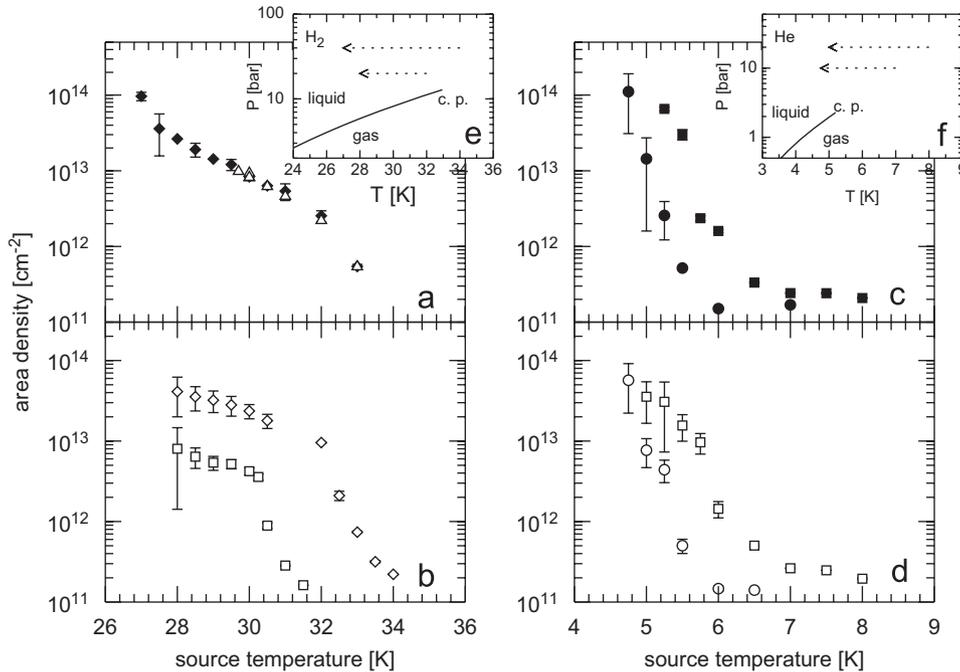
Fig. 2. Area densities of the hydrogen (a) and (b) and helium (c) and (d) liquid beams determined from dump pressure data, Eqs. (1) and (2), as a function of the source temperature T_0 at $P_0 = 10$ (circle), 20 (square), and 40 bar (diamond). The nozzles had a nominal orifice diameter of 3 (closed symbols) and 5 μm (open symbols). (e) and (f) are the pressure–temperature phase diagrams of hydrogen and helium, respectively, showing the two-phase boundary line ending at the critical point (c.p.). The dotted arrows shown in (e) and (f) indicate the stagnation source conditions investigated during the present experiments. The triangles shown in (a) represent the hydrogen area density as determined from the EC data, Eq. (3).
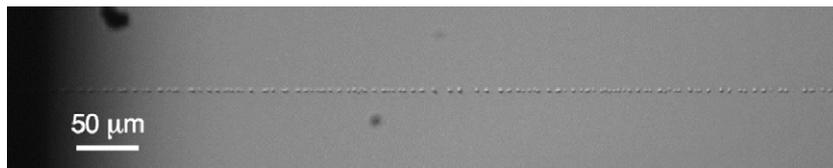
Fig. 3. Image of a Rayleigh droplet stream produced by expanding liquid helium at $P_0 = 6$ bar and $T_0 = 4$ K. The image was recorded with a 2048 × 2048 pixels resolution CCD camera and a 12× zoom lens system. A pulsed laser operating at 532 nm with a pulse width of 8 ns and a repetition rate of 10 Hz was used, coupled to a diffuser, for backside illumination. The nozzle had a nominal diameter $d_0 = 3$ μm.

densities in the source only slightly increase with decreasing T_0 in the temperature ranges investigated here [18], the observed increase in the area density is consistent with the expected exponential narrowing of the liquid beam as a function of the source temperature [11].

Fluctuations in the dump pressure by up to one order of magnitude were invariably observed at lower source temperatures than those displayed in Fig. 2. These density variations in time can be explained by mechanical vibrations at the source and/or by skimmer misalignment along the target beam axis that eventually start playing a role as the liquid beam further narrows at lower source temperatures [11]. We believe that internal target densities even higher than those reported here could be achieved by a more careful design of the differential vacuum chambers and pumping system. Our claim is supported by the additional investigations of liquid helium beams by means of shadow-imaging techniques [17] in a nearly vibration-free test apparatus. Fig. 3 shows a picture of a microscopic, monodirectional stream of about 5 μm diameter liquid helium droplets produced as a result of Rayleigh-oscillation-induced breakup of a liquid He jet expanding from a 3 μm diameter nozzle at $P_0 = 6$ bar and $T_0 = 4$ K. The expected area density corresponding to the beam shown in Fig. 3 is $\sim 10^{16}$ cm^{-2} [14,15], with the interaction length Δx much smaller than 1 mm.

To check the reliability of Eq. (1) we additionally investigated the electron capture (EC) process in collisions of the hydrogen target beam with 150 MeV/u Xe^{54+} ions. If $\dot{N}_{EC}$ is the down-charged ion rate, as measured with a position-sensitive particle detector located further downstream from the interaction region, the area density can be determined from $\dot{N}_{EC}$ according to

$$\dot{N}_{EC} = \sigma \dot{N}_{ion} n \Delta x \qquad (3)$$

where $\dot{N}_{ion}$ is the ion production rate and σ is the total EC cross-section. The EC cross-section, which for low-Z targets and relativistic ion energies ($\gtrsim 10$ MeV/u) coincides essentially with the radiative electron capture (REC) cross-section [3], is known with high accuracy for a wide range of ion species and energies from extensive experimental investigations of recombination processes in relativistic collisions of highly charged ions with neutral low-Z targets (for a review, see Ref. [3] and references therein). In the present case $\sigma \approx 8 \times 10^{-23}$ cm^2 for the hydrogen target. The H$_2$ internal target densities extracted from the EC data according to Eq. (3) are shown as triangles in Fig. 2(a) for source temperatures $T_0 = 29.7-33$ K. The good agreement between the two data sets confirms thus the validity of Eqs. (1) and (2) for the area density determination, and demonstrates that the REC process provides a powerful method for luminosity monitoring in experiments at storage rings.
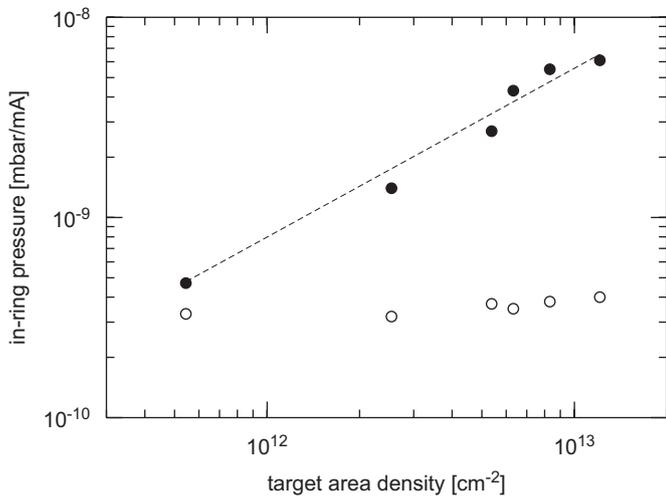
Fig. 4. In-ring pressure measured as a function of the hydrogen area density prior to ion-beam injection (open symbols) and during the interaction with 150 MeV/u Xe^{54+} ions (closed symbols). The dashed line is a fit to the experimental data (see text for details). The H_2 liquid beam was produced at $P_0 = 40$ bar and $T_0 = 29.7-33$ K.

Fig. 4 shows the in-ring pressure, measured about 3 m upstream from the interaction region, as a function of the area density during the interaction of the hydrogen droplet beam with 150 MeV/u Xe^{54+} ions. To account for variations in the ion-beam production rate between successive injections, the in-ring pressures displayed in Fig. 4 by the closed symbols are relative to the ion current, which was in the range 1 ± 0.2 mA. For comparison, we also show by the open symbols the pressure recorded prior to each ion-beam injection. One can see that in the former case the in-ring pressure is substantially larger and, up to a constant, increases as $\approx (n\Delta x)^{0.9}$ in the area density range investigated here, as shown by the dashed line, reaching the largest recorded value of $\approx 6 \times 10^{-9}$ mbar/mA at $n\Delta x \approx 10^{13}$ cm^{-2}. The observed increase in the gas load is attributed to the growth in droplet size with decreasing source temperature. By assuming a H_2 mean droplet size of 100 nm, as determined from Mie light scattering experiments performed under similar source conditions [20] and corresponding to the highest density of 10^{13} cm^{-2} displayed in Fig. 4, it turns out that on average a droplet is hit ≈ 1.1 times during the ≈ 8.5 μs flight time across the 3 mm wide xenon beam with an ion density of $\approx 1.15 \times 10^9$ cm^{-2} under the present experimental conditions. Multiple ion-droplet collisions are expected at lower source temperatures, i.e., at higher target densities, as the droplets further grow in size [20]. Eventually, under laminar-flow conditions micrometer-sized droplets are produced (see Fig. 3), for which collision rates more than two orders of magnitude higher are expected. Further experiments are here needed to investigate the gas load in the interaction region under such extreme collisional conditions.

In conclusion, the present experiments show that the expansion of the liquid into vacuum through sub-10 μm diameter nozzles might represent a valid alternative to the state-of-the-art molecular-beam techniques for producing a high-density internal target for the low-Z gases hydrogen and helium. The highest area density achieved here is comparable with previous results for hydrogen and represents an improvement by several orders of magnitude for the helium target. A major drawback is the observed pressure increase in the interaction region, especially at the higher target densities investigated here, which is probably due to droplet fragmentation upon collisions with the ion beam. This gas load is expected to be even more dramatic with the helium target beam, due to the reduced pumping speed for the He gas. To address the latter issue will necessarily require a differentially pumped interaction chamber. From the physical point of view, the nature of the heating mechanism leading to droplet explosion in relativistic collisions with highly charged ions is particularly appealing, as in some respects it may resemble that occurring in intense ultra-short laser-cluster interactions. In this regard the use of cryogenically cooled liquid droplet beams in a storage ring might open the route to the investigation of fully unexplored collision phenomena.

References

[1] C. Ekström, Nucl. Instr. and Meth. A 362 (1995) 1.
[2] ⟨www.gsi.de/fair/experiments/NUSTAR/Proposals.htm⟩.
[3] J. Eichler, Th. Stöhlker, Phys. Rep. 439 (2007) 1.
[4] C. Morningstar, M.J. Peardon, AIP Conf. Proc. 688 (2004) 220.
[5] H. Reich, W. Bourgeois, B. Franzke, A. Kritzer, V. Varentsov, Nucl. Phys. A 626 (1997) 417c.
[6] H. Dombrowski, D. Grzonka, W. Hamsink, A. Khoukaz, T. Lister, R. Santo, Nucl. Phys. A 626 (1997) 427c.
[7] A. Khoukaz, T. Lister, C. Quentmeier, R. Santo, C. Thomas, Eur. Phys. J. D 5 (1999) 275.
[8] A. Krämer, A. Kritzer, H. Reich, Th. Stöhlker, Nucl. Instr. and Meth. B 174 (2001) 205.
[9] H.J. Stein, M. Hartmann, I. Keshelashvili, Y. Maeda, C. Wilkin, S. Dymov, A. Kacharava, A. Khoukaz, B. Lorentz, R. Maier, T. Mersmann, S. Mikirtychiants, D. Prasuhn, R. Stassen, H. Stockhorst, H. Ströher, Yu Valdau, P. Wüstner, Phys. Rev. Spec. Top. Accel. Beams 11 (2008) 052801.
[10] A. Khoukaz, private communication.
[11] R.E. Grisenti, J.P. Toennies, Phys. Rev. Lett. 90 (2003) 234501.
[12] J. Eggers, E. Villermaux, Rep. Prog. Phys. 71 (2008) 036601.
[13] B. Trostell, Nucl. Instr. and Meth. A 362 (1995) 41.
[14] Ö. Nordhage, Z.K. Li, C.J. Fridén, G. Norman, U. Wiedner, Nucl. Instr. and Meth. A 546 (2005) 391.
[15] A.V. Boukharov, M. Büscher, A.S. Gerasimov, V.D. Chernetsky, P.V. Fedorets, I.N. Maryshev, A.A. Semenov, A.F. Ginevskii, Phys. Rev. Lett. 100 (2008) 174505.
[16] U. Saalmann, Ch. Siedschlag, J.M. Rost, J. Phys. B 39 (2006) R39.
[17] R.E. Grisenti, R.A. Costa Fraga, N. Petridis, R. Dörner, J. Deppe, Europhys. Lett. 73 (2006) 540.
[18] ⟨webbook.nist.gov/chemistry/fluid/⟩.
[19] H. Buchenau, E.L. Knuth, J. Northby, J.P. Toennies, C. Winkler, J. Chem. Phys. 92 (1990) 6875.
[20] R.A. Costa Fraga, R.E. Grisenti, unpublished results.